Journal of Physics: Condensed Matter

PAPER

Optical response of a quantum dot–metal nanoparticle hybrid interacting with a weak probe field

J. Phys.: Condens. Matter **25** (2013) 045304 (10pp) doi:10.1088/0953-8984/25/4/045304

Optical response of a quantum dot–metal nanoparticle hybrid interacting with a weak probe field

Spyridon G Kosionis[1], **Andreas F Terzis**[1], **Seyed M Sadeghi**[2] **and Emmanuel Paspalakis**[3]

[1] Physics Department, School of Natural Sciences, University of Patras, Patras 265 04, Greece
[2] Department of Physics, University of Alabama in Huntsville, Huntsville, AL 35899, USA
[3] Materials Science Department, School of Natural Sciences, University of Patras, Patras 265 04, Greece

E-mail: paspalak@upatras.gr

Received 17 November 2012
Published 20 December 2012
Online at stacks.iop.org/JPhysCM/25/045304

Abstract

We study optical effects in a hybrid system composed of a semiconductor quantum dot and a spherical metal nanoparticle that interacts with a weak probe electromagnetic field. We use modified nonlinear density matrix equations for the description of the optical properties of the system and obtain a closed-form expression for the linear susceptibilities of the quantum dot, the metal nanoparticle, and the total system. We then investigate the dependence of the susceptibility on the interparticle distance as well as on the material parameters of the hybrid system. We find that the susceptibility of the quantum dot exhibits optical transparency for specific frequencies. In addition, we show that there is a range of frequencies of the applied field for which the susceptibility of the semiconductor quantum dot leads to gain. This suggests that in such a hybrid system quantum coherence can reverse the course of energy transfer, allowing flow of energy from the metallic nanoparticle to the quantum dot. We also explore the susceptibility of the metal nanoparticle and show that it is strongly influenced by the presence of the quantum dot.

(Some figures may appear in colour only in the online journal)

1. Introduction

The optical properties of complex nanosystems that combine semiconductor quantum dots (SQDs) and plasmonic nanostructures, such as spherical metallic nanoparticles (MNPs) and metallic nanorods, have attracted significant interest in recent years. The placement of the SQD next to plasmonic nanostructures leads to significant alteration of the electromagnetic field felt by the quantum systems due to the interaction between the excitons from the SQD and the surface plasmons of the metallic nanostructures. This has significant influence on the optical properties of the hybrid complexes, and leads to several interesting phenomena, for example, the creation of controlled Rabi oscillations [1, 2], plasmonic meta-resonances [2], tunable ultrafast nanoswitches [3], modified resonance fluorescence and photon statistics [4, 5], and intrinsic optical bistability [6] in SQD–MNP hybrid systems.

In addition, the nonlinear optical response of SQD–MNP complexes and the creation of controlled slow light [7], gain without inversion [8] and optical bistability [9] under the interaction of a weak probe field and a strong pump field have been studied. Furthermore, it has recently been shown [10] that the combination of SQD–MNP hybrids that are coupled by a weak probe field, a strong pump field and nanomechanical resonators has the potential to lead to ultrasensitive mass detection.

In all of these studies the optical response of the probe field is studied solely by the optical susceptibility of the SQD. In fact, in the absence of the pump field it has been shown that the linear absorption spectrum of an SQD–MNP hybrid system has a Lorenzian form and its width and height is strongly dependent on the distance between the SQD and the MNP.

In this work we calculate and analyze the linear optical susceptibility of an SQD–MNP hybrid system. The hybrid complex that we study is comprised of a spherical MNP and a small SQD. The SQD is described by a two-level system and the interaction of the system with an external laser field is described by the modified nonlinear density matrix equations that take into account the interaction between excitons and surface plasmons [11–13]. This methodology has recently been used in such systems, or in directly related systems that contain plasmonic nanorods and multi-level quantum dots, for the analysis of their optical properties [1–10] and for the study of energy absorption and the creation of the nonlinear Fano effect in energy absorption [11–22].

Here, we present approximate analytical solutions of the nonlinear density matrix equations and use these solutions for the determination of the linear optical susceptibilities of the SQD, the MNP and the total system. We find that the linear optical susceptibility of the SQD leads to an absorption spectrum that is not Lorenzian. The absorption spectrum can become zero for specific frequencies and even negative, so gain without inversion is possible for a range of frequencies. In addition, we show that the linear susceptibility of the MNP is strongly influenced by the presence of the SQD. We find that both the SQD and the MNP susceptibilities contribute to the optical properties of the hybrid system. We investigate the dependence of the linear optical susceptibilities of the SQD, the MNP and the total system on the interparticle distance as well as on material parameters of the hybrid system. Actually, all of these effects occur due to the strong exciton–plasmon coupling and do not need the use of additional external (coherent or incoherent) fields.

Note that the negative absorption in the SQD spectrum predicted here is different from that predicted in another publication in the same system by one of us [8], as there the gain in the probe field occurs under the influence of a strong pump field. In this paper, however, no external pumping field is used, and the gain occurs due to energy transfer from the MNP to the SQD. This is an important result, as it suggests that the quantum coherence generated in the SQD–MNP system can reverse the course of energy transfer as dictated by Förster energy transfer [15].

2. Calculation of the susceptibilities

We consider a hybrid structure composed of a spherical MNP of radius a and a spherical SQD with radius b, in an environment with dielectric constant ε_{env}, as shown in figure 1. The center-to-center distance between the two particles is represented by R. We also assume that the radius of the SQD is much smaller than the radius of the MNP and also consider that $R > a$. This system interacts with an oscillating electromagnetic field $E(t) = E_0 \cos(\omega t)$, applied along the $\hat{z}$ direction, which excites the interband transition between the two energy levels of the SQD $|1\rangle \to |2\rangle$, with exciton energy equal to $\hbar\omega_0$. Only these two levels contribute to the dynamics of the system and an oscillating dipole moment is induced. The dielectric constant of the SQD is represented by ε_{S}, while we treat the MNP as a classical dielectric particle with dielectric function $\varepsilon_{\text{m}}(\omega)$.

The electromagnetic field also excites plasmons on the surface of the MNP. These plasmonic excitations provide a strong continuous spectral response. Such surface plasmons influence the excitons and induce dipole–dipole interaction between excitons and plasmons [11]. This interaction is responsible for the coupling between the two particles and leads to Förster energy transfer [15]. Taking into account the symmetry of the SQD and assuming that the electromagnetic field is linearly polarized, the Hamiltonian of the system takes the form

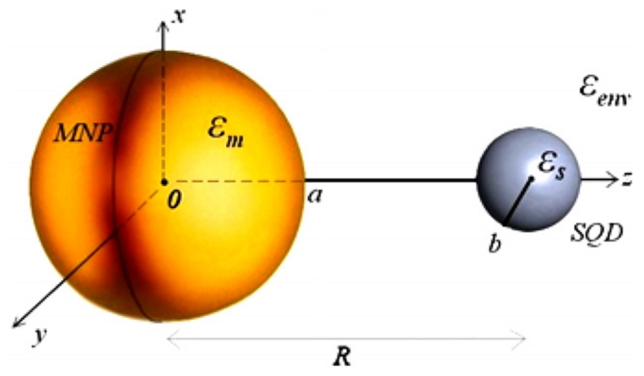

Figure 1. The hybrid system constitutes of an SQD of radius b which is coupled to an MNP of radius a. The centers of the two particles are separated by a distance represented by R.

$$H = \hbar\omega_0 |2\rangle\langle 2| - \mu E_{\text{SQD}} \left(|1\rangle\langle 2| + |2\rangle\langle 1|\right), \tag{1}$$

where μ represents the dipole moment of the SQD corresponding to the single exciton transition, and E_{SQD} represents the electric field inside the SQD, which is explicitly written as [12, 13]:

$$E_{\text{SQD}} = \frac{\hbar}{\mu}[(\Omega + G\sigma)\,\mathrm{e}^{-\mathrm{i}\omega t} + \left(\Omega^* + G^*\sigma^*\right)\mathrm{e}^{\mathrm{i}\omega t}]. \tag{2}$$

We introduce the slowly varying quantities $\sigma = \rho_{21}\mathrm{e}^{\mathrm{i}\omega t}$ and $\sigma^* = \rho_{12}\mathrm{e}^{-\mathrm{i}\omega t}$, with ρ_{ij} being the density matrix elements. We also define the parameters Ω and G respectively as [12, 13]

$$\Omega = \frac{E_0\mu}{2\hbar\varepsilon_{\text{effS}}}\left(1 + \frac{s_a\gamma_1 a^3}{R^3}\right) \quad \text{and}$$
$$G = \sum_{n=1}^{N} \frac{1}{4\pi\varepsilon_{\text{env}}} \frac{(n+1)^2\gamma_n a^{2n+1}\mu^2}{\hbar\varepsilon_{\text{effS}}^2 R^{2n+4}}, \tag{3}$$

where $\gamma_n = \frac{\varepsilon_{\text{m}}(\omega) - \varepsilon_{\text{env}}}{\varepsilon_{\text{m}}(\omega) + \frac{n+1}{n}\varepsilon_{\text{env}}}$ and $\varepsilon_{\text{effS}} = \frac{2\varepsilon_{\text{env}} + \varepsilon_{\text{S}}}{3\varepsilon_{\text{env}}}$, with ε_0 being the dielectric constant of the vacuum and $s_a = 2$ as the applied field is parallel to the interparticle axis of the system (z axis). The parameter Ω is related to the direct coupling to the applied field (first term), as well as to the field from the MNP that is induced by the applied field (second term). The parameter G represents the self-interaction of the SQD. This arises from the procedure described below. At first, the electromagnetic field polarizes the SQD, which in turn polarizes the MNP. The MNP then produces a field that interacts with the SQD (dipole effect). However, in this study, we are aiming to be more precise and thus take into account multipole effects [12]. Below, we will take $N = 10$ in our calculations, as we find that this is enough for obtaining converging results.

Our goal is to obtain an analytical expression for the first order susceptibility $\chi^{(1)}$ of the system in a straightforward manner. This is given by the sum of the first order susceptibility of the SQD, χ_{SQD}, and the first order susceptibility of the MNP, χ_{MNP}. We initially derive an expression for the first order susceptibility that determines the optical response of the SQD [7–9]. For this we derive the density matrix equations, which describe the dynamics of the system. These under the rotating wave approximation are given by [11–13]

$$\dot{\sigma}(t) = -\frac{1}{T_2}\sigma(t) + \mathrm{i}\Omega\Delta(t) + \mathrm{i}G\Delta(t)\sigma(t) + \mathrm{i}\delta\sigma(t), \tag{4}$$

$$\dot{\Delta}(t) = 2\mathrm{i}\Omega^*\sigma(t) - 2\mathrm{i}\Omega\sigma^*(t) + 4G_{\mathrm{I}}\sigma(t)\sigma^*(t) - \frac{\Delta(t)-1}{T_1}. \tag{5}$$

In equations (4) and (5) $\Delta(t) = \sigma_{11}(t) - \sigma_{22}(t)$ corresponds to the population difference between the two energy levels, which is a real quantity, $\delta = \omega - \omega_0$ is the detuning of the applied field from resonance and G_{I} represents the imaginary part of the parameter G. Moreover, T_1 is the population relaxation time, while T_2 is the relaxation due to dephasing processes of the SQD under the presence of the MNP. The relaxation time T_1, and thus the relaxation time T_2, are also influenced by the presence of the MNP [23–26]. However, for the parameters that we use here the values of T_1, T_2 do not practically change in the frequency region of interest, and therefore will be considered constant in this study, as in previous papers concerning similar systems [1–21].

From equation (4) in the steady state we obtain

$$\sigma = -\frac{\Omega\Delta}{\delta + G\Delta + \mathrm{i}/T_2}. \tag{6}$$

If we substitute equation (6) in (5), solve the last one in the steady state and approximate Δ at first order according to perturbation theory, we find that $\Delta \approx 1$. As $\chi_{\mathrm{SQD}} = \frac{2\Gamma}{\varepsilon_0 E_0 V}\mu\sigma$, where Γ is the optical confinement factor and V is the volume of the SQD [27], we obtain the following analytical expression for the linear susceptibility of the SQD:

$$\chi_{\mathrm{SQD}} = -\frac{\Gamma}{V}\frac{\mu^2\kappa T_2}{\hbar\varepsilon_0}\frac{T_2(\delta + G_{\mathrm{R}}) - \mathrm{i}(1 + T_2 G_{\mathrm{I}})}{\left[(1+T_2G_{\mathrm{I}})^2 + T_2^2(\delta + G_{\mathrm{R}})^2\right]}, \tag{7}$$

where $\kappa = \left(1 + s_a\gamma_1 a^3/R^3\right)/\varepsilon_{\mathrm{effS}}$.

Then, we determine the first order optical susceptibility of the MNP. The polarization of the MNP is written as [12]

$$P_{\mathrm{MNP}} = P_{\mathrm{MNP}}^{(+)}\mathrm{e}^{-\mathrm{i}\omega t} + \mathrm{c.c.}, \tag{8}$$

where

$$P_{\mathrm{MNP}}^{(+)} = 3\varepsilon_{\mathrm{env}}\gamma_1\left[\frac{E_0}{2} + \frac{1}{4\pi\varepsilon_{\mathrm{env}}}\frac{s_a\mu\sigma}{\varepsilon_{\mathrm{effS}}R^3}\right]. \tag{9}$$

As $\chi_{\mathrm{MNP}} = \frac{2}{\varepsilon_0 E_0}P_{\mathrm{MNP}}^{(+)}$ we obtain

$$\chi_{\mathrm{MNP}} = 3\gamma_1\left[\frac{\varepsilon_{\mathrm{env}}}{\varepsilon_0} - \frac{1}{4\pi\varepsilon_0\varepsilon_{\mathrm{effS}}}\frac{s_a\mu^2\kappa T_2}{\hbar R^3} \times \frac{T_2(\delta + G_{\mathrm{R}}) - \mathrm{i}(1+T_2G_{\mathrm{I}})}{[(1+T_2G_{\mathrm{I}})^2 + T_2^2(\delta+G_{\mathrm{R}})^2]}\right]. \tag{10}$$

In the case where the frequency range of interest is such that the parameters $\gamma_1 = \gamma_{1R} + \mathrm{i}\gamma_{1I}$, $\kappa = \kappa_{\mathrm{R}} + \mathrm{i}\kappa_{\mathrm{I}}$ and $G = G_{\mathrm{R}} + \mathrm{i}G_{\mathrm{I}}$ are practically independent of the frequency, we can easily estimate from equation (7) the values of several characteristic features of the real and imaginary part of the susceptibility of the SQD. Hence, as far as the real part is concerned, we find that it becomes zero when

$$\delta = -G_{\mathrm{R}} - \frac{\kappa_{\mathrm{I}}}{\kappa_{\mathrm{R}}}\left(\frac{1}{T_2} + G_{\mathrm{I}}\right), \tag{11}$$

and has its maximum and minimum values when

$$\delta_{\max} = -G_{\mathrm{R}} - \left(\frac{1}{T_2} + G_{\mathrm{I}}\right)\left[\frac{\kappa_{\mathrm{I}}}{\kappa_{\mathrm{R}}} + \left[1 + \left(\frac{\kappa_{\mathrm{I}}}{\kappa_{\mathrm{R}}}\right)^2\right]^{1/2}\right], \tag{12}$$

and

$$\delta_{\min} = -G_{\mathrm{R}} - \left(\frac{1}{T_2} + G_{\mathrm{I}}\right)\left[\frac{\kappa_{\mathrm{I}}}{\kappa_{\mathrm{R}}} - \left[1 + \left(\frac{\kappa_{\mathrm{I}}}{\kappa_{\mathrm{R}}}\right)^2\right]^{1/2}\right]. \tag{13}$$

That is, it is shifted with respect to the value of the detuning at which the real part becomes zero by $(\frac{1}{T_2} + G_{\mathrm{I}})[1 + (\frac{\kappa_{\mathrm{I}}}{\kappa_{\mathrm{R}}})^2]^{1/2}$ on both sides (right/left) and hence the gap between the minimum and the maximum is $2(\frac{1}{T_2} + G_{\mathrm{I}})[1 + (\frac{\kappa_{\mathrm{I}}}{\kappa_{\mathrm{R}}})^2]^{1/2}$. Moreover, from equation (7) we conclude that the zero of the imaginary part of the susceptibility of the SQD occurs at

$$\delta = -G_{\mathrm{R}} + \frac{\kappa_{\mathrm{R}}}{\kappa_{\mathrm{I}}}\left(\frac{1}{T_2} + G_{\mathrm{I}}\right). \tag{14}$$

For higher values of the detuning, we have gain in the SQD, and this gain is without population inversion. The maximum and minimum peaks of the imaginary part respectively arise at

$$\delta_{\max} = -G_{\mathrm{R}} + \left(\frac{1}{T_2} + G_{\mathrm{I}}\right)\left[\frac{\kappa_{\mathrm{R}}}{\kappa_{\mathrm{I}}} - \left[1 + \left(\frac{\kappa_{\mathrm{R}}}{\kappa_{\mathrm{I}}}\right)^2\right]^{1/2}\right], \tag{15}$$

and

$$\delta_{\min} = -G_{\mathrm{R}} + \left(\frac{1}{T_2} + G_{\mathrm{I}}\right)\left[\frac{\kappa_{\mathrm{R}}}{\kappa_{\mathrm{I}}} + \left[1 + \left(\frac{\kappa_{\mathrm{R}}}{\kappa_{\mathrm{I}}}\right)^2\right]^{1/2}\right]. \tag{16}$$

In fact, equations (15) and (16) predict, in the case that $\kappa_{\mathrm{R}} \gg \kappa_{\mathrm{I}}$ which is the usual situation, that the maximum occurs at approximately $\delta \sim -G_{\mathrm{R}}$ and the minimum (which corresponds to the gain dip) at $\delta = -G_{\mathrm{R}} + 2\frac{\kappa_{\mathrm{R}}}{\kappa_{\mathrm{I}}}(\frac{1}{T_2} + G_{\mathrm{I}})$. Finally, we can identify the magnitude of the absorption and the gain peak, which are respectively equal to

$$\mathrm{Im}[\chi_{\mathrm{SQD}}]_{\max} = \frac{\Gamma}{V}\frac{\mu^2 T_2}{\hbar\varepsilon_0}\frac{1}{2(1+T_2G_{\mathrm{I}})}\frac{\kappa_{\mathrm{I}}^2}{[\kappa_{\mathrm{R}}^2 + \kappa_{\mathrm{I}}^2]^{1/2} - \kappa_{\mathrm{R}}}, \tag{17}$$

$$\mathrm{Im}[\chi_{\mathrm{SQD}}]_{\mathrm{min}} = -\frac{\Gamma}{V}\frac{\mu^2 T_2}{\hbar\varepsilon_0}\frac{1}{2\,(1+T_2 G_{\mathrm{I}})}\frac{\kappa_{\mathrm{I}}^2}{[\kappa_{\mathrm{R}}^2+\kappa_{\mathrm{I}}^2]^{1/2}+\kappa_{\mathrm{R}}}. \tag{18}$$

Similarly, in this case of practically frequency-independent parameters, the values of several characteristic features of the real and imaginary part of the MNP susceptibility can be estimated from equation (10) by performing simple calculations to find the roots of the susceptibility and its derivative. However, the analytical expressions for the values of the detuning at which the real and imaginary part of the MNP susceptibility becomes zero are very lengthy and intractable and give practically no more information.

On the other hand, it becomes apparent by comparing equations (7) and (10) that the values of the detuning at which the maximum and minimum values of the susceptibilities occur should have the same functional form. The latter occurs as the derivative of equation (10) is practically the same with the derivative of equation (7), once we replace the parameter κ of equation (7) with the parameter $\tilde{\kappa}(\equiv\kappa\cdot\gamma_1=\tilde{\kappa}_{\mathrm{R}}+\mathrm{i}\tilde{\kappa}_{\mathrm{I}})$. Therefore, in order to estimate the position of the minima and maxima of the real and imaginary susceptibilities we can use equations (12), (13), (15) and (16) by just replacing the parameter κ with the parameter $\tilde{\kappa}$. For example, we show the characteristic values related to the minimum of the imaginary part of the susceptibility to arise at

$$\delta_{\mathrm{min}} = -G_{\mathrm{R}} + \left(\frac{1}{T_2}+G_{\mathrm{I}}\right)\left[\frac{\tilde{\kappa}_{\mathrm{R}}}{\tilde{\kappa}_{\mathrm{I}}} + \left[1+\left(\frac{\tilde{\kappa}_{\mathrm{R}}}{\tilde{\kappa}_{\mathrm{I}}}\right)^2\right]^{1/2}\right], \tag{19}$$

showing a value equal to

$$\mathrm{Im}[\chi_{\mathrm{MNP}}]_{\mathrm{min}} = \frac{3\varepsilon_{\mathrm{env}}}{\varepsilon_0}\gamma_{1I} + \frac{\chi^0_{\mathrm{MNP}}}{2\,(1+T_2 G_{\mathrm{I}})}\frac{\tilde{\kappa}_{\mathrm{I}}^2}{[[\tilde{\kappa}_{\mathrm{R}}^2+\tilde{\kappa}_{\mathrm{I}}^2]^{1/2}+\tilde{\kappa}_{\mathrm{R}}]}, \tag{20}$$

where $\chi^0_{\mathrm{MNP}} \equiv -\frac{3s_a\mu^2 T_2}{4\pi\varepsilon_0\varepsilon_{\mathrm{effS}}\hbar R^3}$.

Following exactly the same reasoning we can get simple expressions for the extreme values and the detuning at which these extreme values occur for the real and imaginary part of the total susceptibility. Hence, for all equations determining these features we get expressions of the same functional form, with proper replacement of the important parameter κ. In order to clarify what changes are needed for the expressions in the total susceptibility, we present the characteristic values of the detuning at which occurs the minimum of the imaginary part of the susceptibility and the minimum value:

$$\delta_{\mathrm{min}} = -G_{\mathrm{R}} + \left(\frac{1}{T_2}+G_{\mathrm{I}}\right)\left[\frac{(|\chi^0_{\mathrm{SQD}}|\kappa_{\mathrm{I}}+|\chi^0_{\mathrm{MNP}}|\tilde{\kappa}_{\mathrm{I}})}{(|\chi^0_{\mathrm{SQD}}|\kappa_{\mathrm{R}}+|\chi^0_{\mathrm{MNP}}|\tilde{\kappa}_{\mathrm{R}})} + \left[1+\left(\frac{(|\chi^0_{\mathrm{SQD}}|\kappa_{\mathrm{I}}+|\chi^0_{\mathrm{MNP}}|\tilde{\kappa}_{\mathrm{I}})}{(|\chi^0_{\mathrm{SQD}}|\kappa_{\mathrm{R}}+|\chi^0_{\mathrm{MNP}}|\tilde{\kappa}_{\mathrm{R}})}\right)^2\right]^{1/2}\right], \tag{21}$$

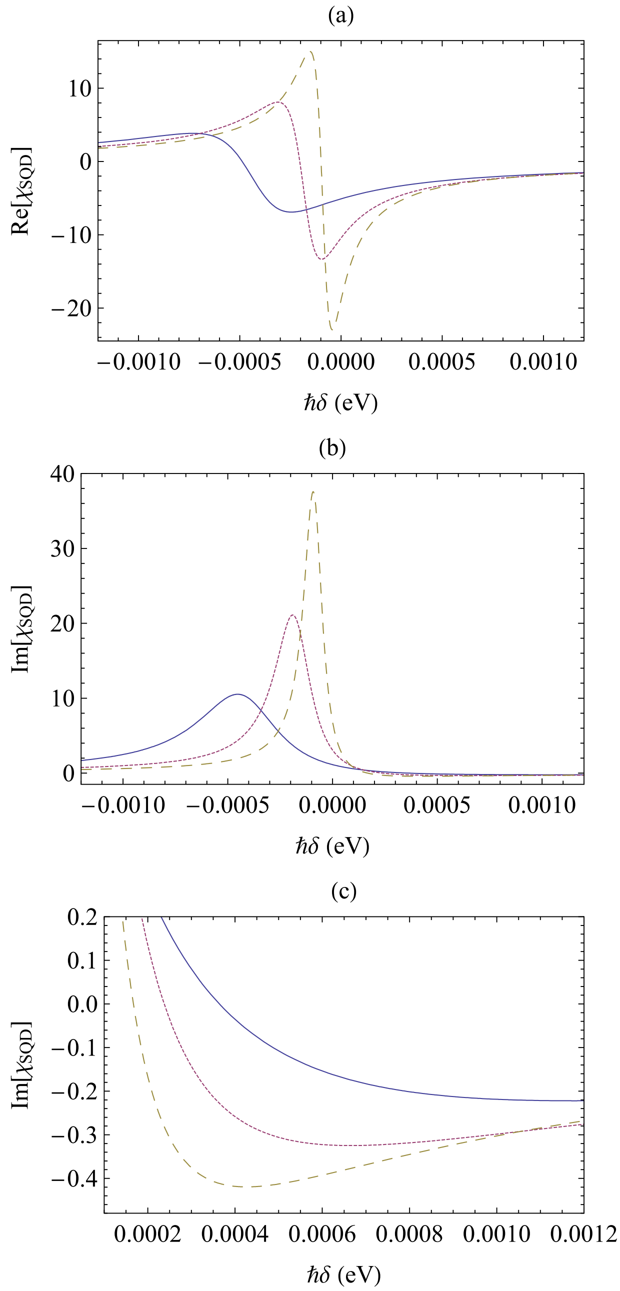

Figure 2. The spectral form of the real, (a), and imaginary part, (b) and (c), of the linear susceptibility of the SQD, χ_{SQD}, as a function of the detuning $\hbar\delta$ of the probe field for several values of the interparticle distance: $R = 11$ nm (solid curve), 12 nm (dotted curve) and 13 nm (dashed curve). The rest parameters are $\Gamma/V = 5\times10^{23}\ \mathrm{m}^{-3}$, $a = 7.5$ nm, $T_2 = 0.3$ ns, $\varepsilon_{\mathrm{env}} = \varepsilon_0$, $\varepsilon_{\mathrm{S}} = 6\varepsilon_0$, $\hbar\omega_0 = 2.5$ eV and $\mu = 0.65e$ nm.

$$\begin{aligned}\mathrm{Im}[\chi^{(1)}]_{\mathrm{min}} = {} & \frac{3\varepsilon_{\mathrm{env}}}{\varepsilon_0}\gamma_{1I} - ((|\chi^0_{\mathrm{SQD}}|\kappa_{\mathrm{I}}+|\chi^0_{\mathrm{MNP}}|\tilde{\kappa}_{\mathrm{I}})^2) \\ & \times (2(1+T_2G_{\mathrm{I}})[[(|\chi^0_{\mathrm{MNP}}|\tilde{\kappa}_{\mathrm{R}}+|\chi^0_{\mathrm{SQD}}|\kappa_{\mathrm{R}})^2 \\ & + (|\chi^0_{\mathrm{SQD}}|\kappa_{\mathrm{I}}+|\chi^0_{\mathrm{MNP}}|\tilde{\kappa}_{\mathrm{I}})^2]^{1/2} \\ & + (|\chi^0_{\mathrm{MNP}}|\tilde{\kappa}_{\mathrm{R}}+|\chi^0_{\mathrm{SQD}}|\kappa_{\mathrm{R}})])^{-1},\end{aligned} \tag{22}$$

where $\chi^0_{\mathrm{SQD}} \equiv -\frac{\Gamma}{V}\frac{\mu^2 T_2}{\hbar\varepsilon_0}$.

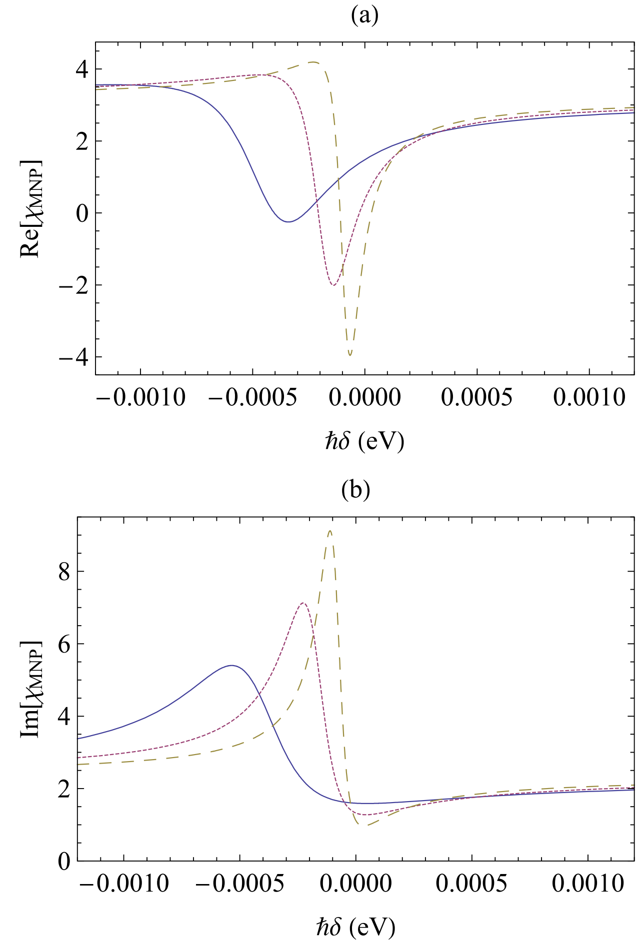

Figure 3. The spectral form of the real, (a), and imaginary part, (b), of the linear susceptibility of the MNP, $\chi_{\rm MNP}$, as a function of the detuning $\hbar\delta$ of the applied field for the same parameters as in figure 2. The interparticle distance is $R = 11$ nm (solid curve), 12 nm (dotted curve) and 13 nm (dashed curve).

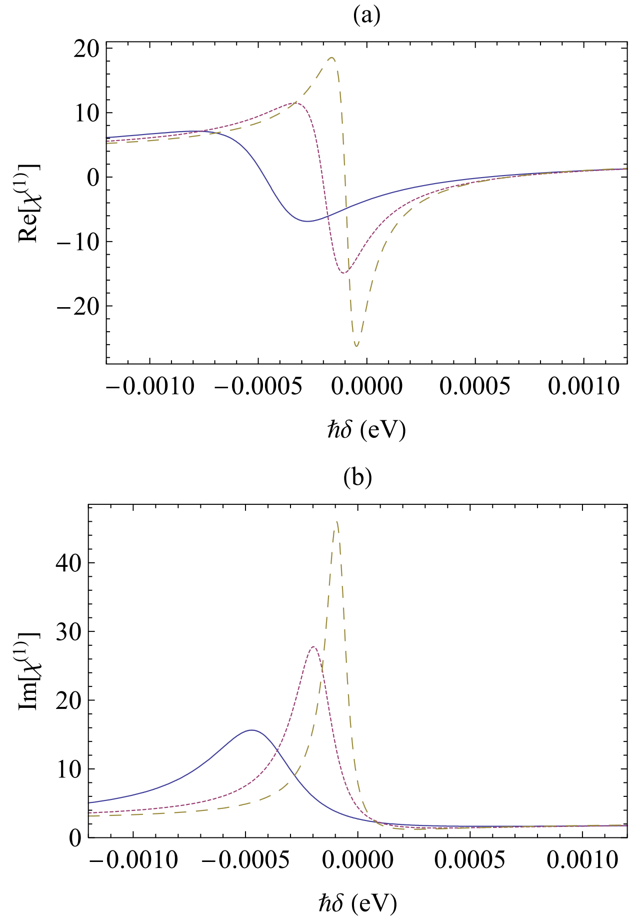

Figure 4. The spectral form of the real, (a), and imaginary part, (b), of the total susceptibility, $\chi^{(1)}$, as a function of the detuning $\hbar\delta$ of the applied field for the same parameters as in figure 2. The interparticle distance is $R = 11$ nm (solid curve), 12 nm (dotted curve) and 13 nm (dashed curve).

We note that the MNP plays a crucial role in the gain without inversion, as due to the interaction between the excitons of the SQD and the surface plasmons of the MNP, energy is transferred from the MNP to the SQD, and this makes gain without inversion possible.

3. Form of the susceptibilities

In the following we present results for the spectral form of the linear susceptibility. Initially, in figures 2–7, we take the dephasing times to be $T_2 = 0.3$ ns as in previous studies, see e.g. [2, 3, 6, 10–13, 15]. The dielectric constants take different values for the environment and the SQD. Here, we consider that $\varepsilon_{\rm S} = 6\varepsilon_0$ and $\varepsilon_{\rm env} = \varepsilon_0$, where ε_0 is the dielectric constant of the vacuum. In the strongly confined regime for the SQD, we take $\Gamma/V = 5 \times 10^{23}$ m^{-3}. Moreover, for the dielectric function $\varepsilon_{\rm m}(\omega)$ of the MNP we use the experimental values that correspond to the case of gold, according to [28]. The interband optical transition matrix element is $\mu = 0.65e$ nm, while the energy gap between the two levels that contribute to the dynamics is $\hbar\omega_0 = 2.5$ eV at the plasmon peak of the MNP. These parameters have been used in various studies, see e.g. [2, 3, 6, 10–13, 15], and correspond to colloidal SQDs (typically CdSe [6]).

In figures 2–7 we study the dependence of the linear susceptibilities of the SQD, the MNP and the total system on the center-to-center distance between the SQD and the MNP. Figures 2–4 correspond to several low values of the parameter R, while figures 5–7 depict higher values of it. In all figures, the susceptibilities are plotted as a function of the detuning $\hbar\delta\,[=\hbar(\omega - \omega_0)]$ of the probe field, while we consider the radius of the metal nanoparticle to be $a = 7.5$ nm.

In all these figures 2–7 the previously mentioned features, described by equations (11)–(22), are observed at positions and take values described by these expressions, as in this range of interest γ_1, κ, G are almost constant. Moreover, as $1/T_2 = 3.34$ ns^{-1}, in all cases studied in figures 2–4 the $1/T_2$ term is much smaller than the real and imaginary part of G and its contribution can be considered of minor importance (i.e. in most cases it can be practically ignored).

Then, we discuss in more detail the results obtained for longer interparticle distance (shown in figures 5–7). In this case, the range of interest is very narrow and to an excellent approximation the G-parameter is constant. Contrary to the previously discussed figures 2–4 the parameter

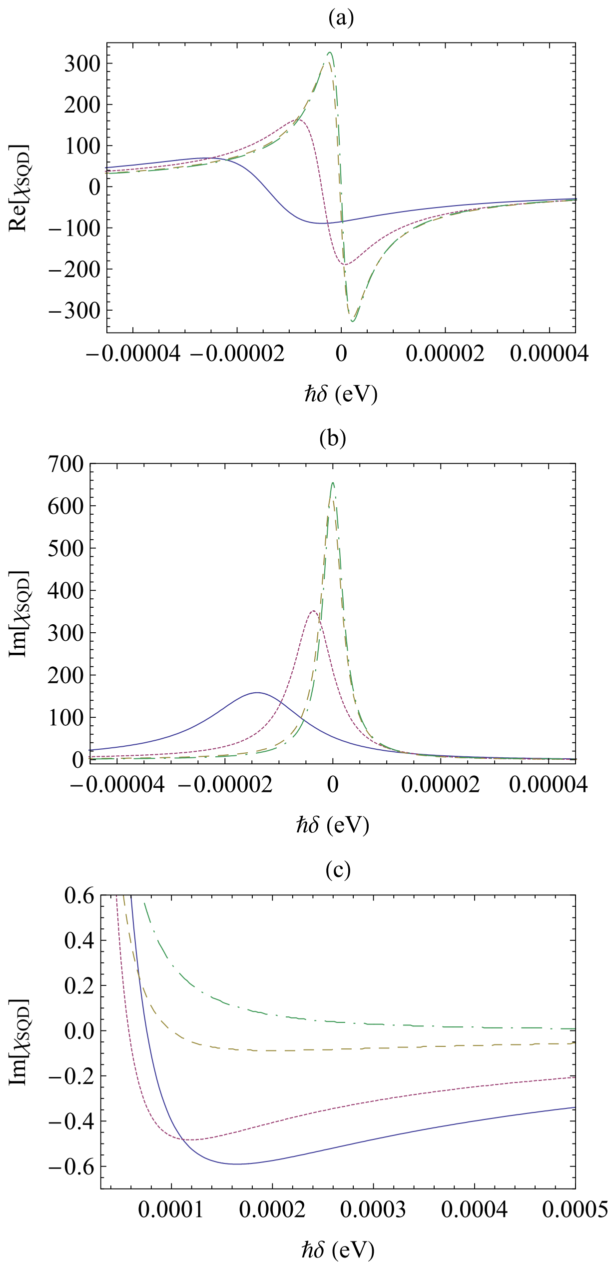

Figure 5. The same as in figure 2, for different values of the interparticle distances $R = 16.5$ nm (solid curve), 20 nm (dotted curve), 30 nm (dashed curve) and 80 nm (dashed–dotted curve).

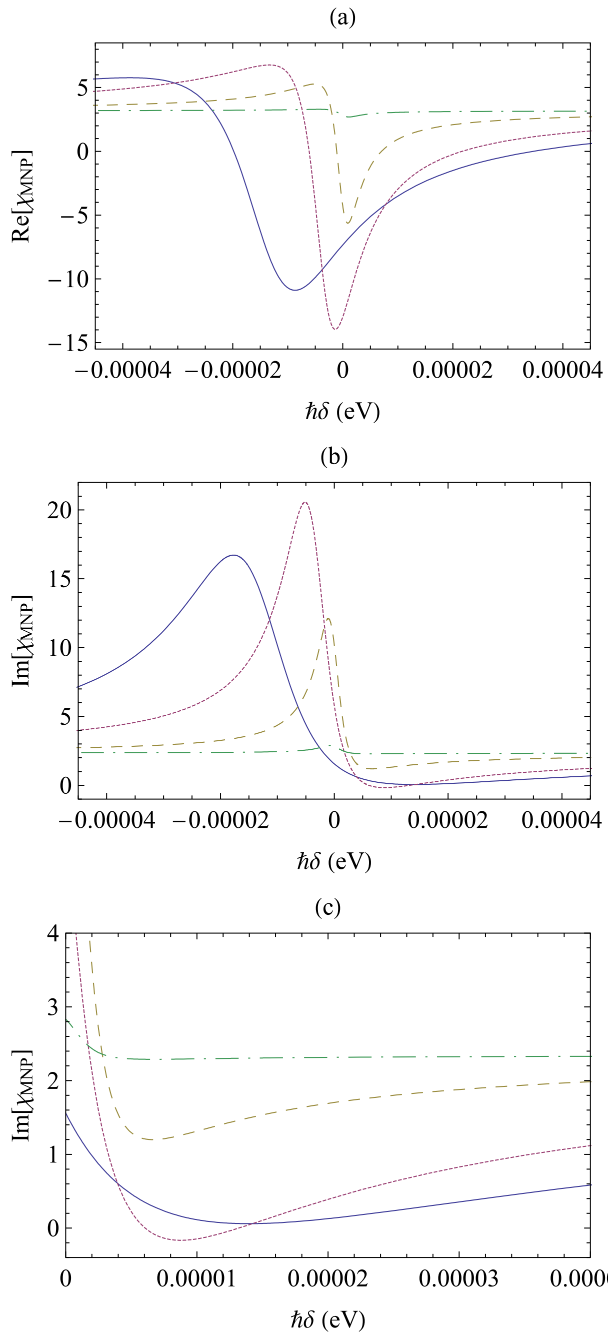

Figure 6. The same as in figure 5 but for χ_{MNP}. The interparticle distance is $R = 16.5$ nm (solid curve), 20 nm (dotted curve), 30 nm (dashed curve) and 80 nm (dashed–dotted curve).

$1/T_2$(=3.34 ns^{-1}) is now very important in the explanation of the observed features, as G has comparable or smaller values when compared to $1/T_2$. All the features that characterize these figures are explained by means of the equations (11)–(22). However, for high interparticle distances, the imaginary part of the κ-parameter is rather small and we get simplified expressions for (a) the value of the detuning at resonance for Re[χ_{SQD}] which is practically equal to $-G_{\mathrm{R}}$ (see equation (11)) and (b) the width (now, the absorption curve is rather symmetric) which is estimated by the simplification of equations (12) and (13) to be approximately equal to $2(\frac{1}{T_2} + G_{\mathrm{I}})$.

In general, we note that the position of this resonance moves towards higher values of the detuning parameter as the parameter R increases. This was expected, since all the three parameters $G_{\mathrm{R}}, G_{\mathrm{I}}, \kappa_{\mathrm{I}}/\kappa_{\mathrm{R}}$ decrease, when the interparticle distance increases. Moreover, as the SQD approaches the MNP, the two sidebands increase in magnitude and shrink in the direction of the detuning (i.e. a decrease of the 'width' arises), while the dispersion at resonance becomes steeper.

The most striking of our findings is that for all values of the interparticle distance (see figures 2–5), we note that the absorption coefficient Im[χ_{SQD}] becomes negative for a

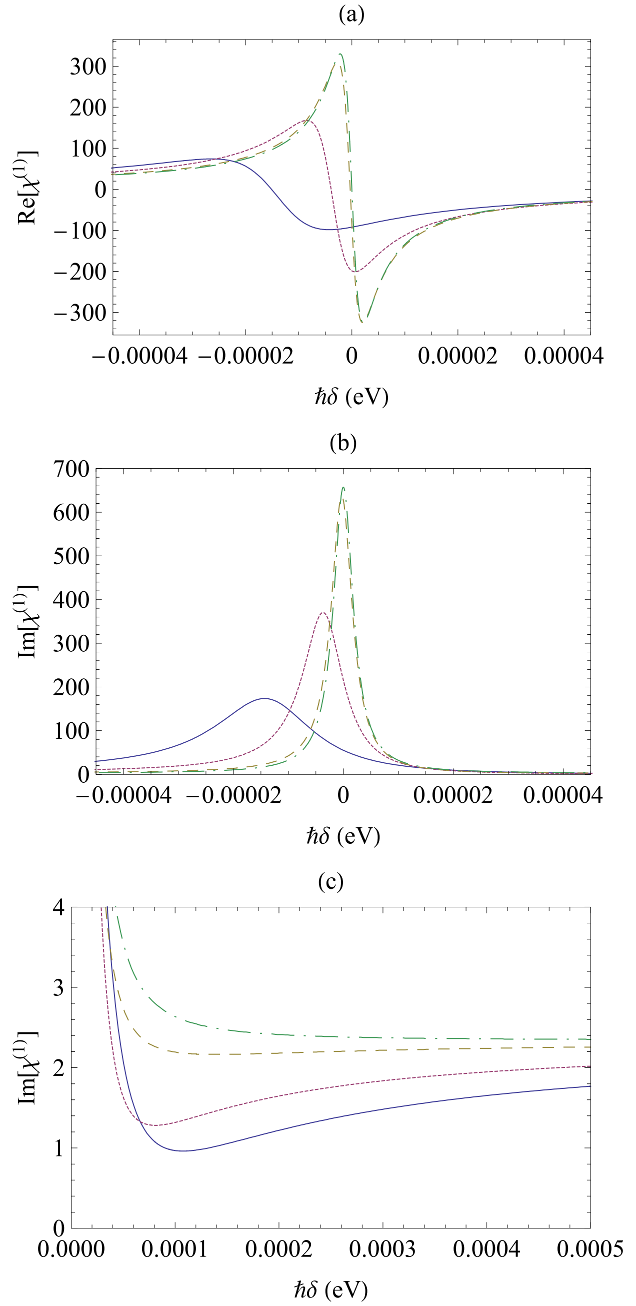

Figure 7. The same as in figure 5 but for $\chi^{(1)}$. The interparticle distance is $R = 16.5$ nm (solid curve), 20 nm (dotted curve), 30 nm (dashed curve) and 80 nm (dashed–dotted curve).

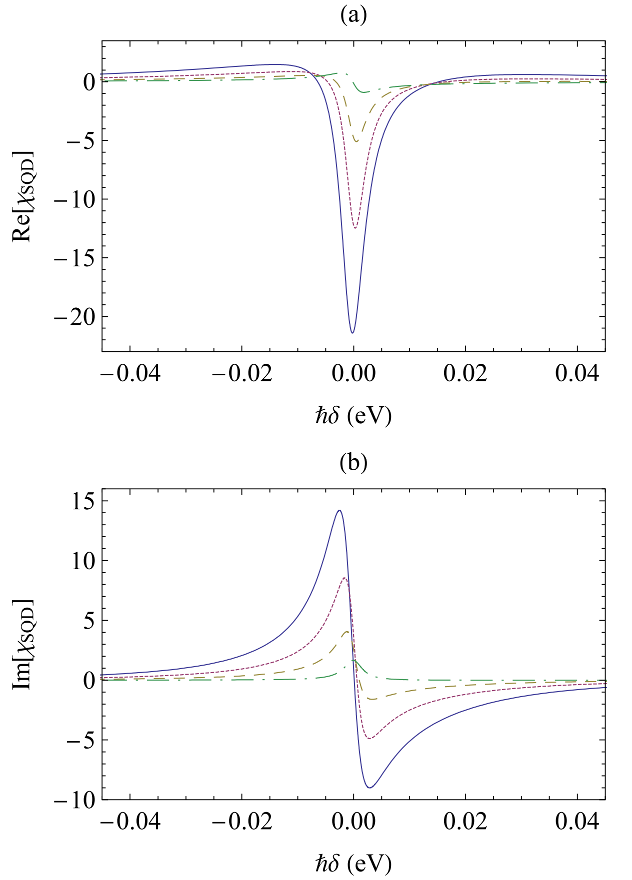

Figure 8. The spectral form of the real, (a), and imaginary part, (b), of the linear susceptibility of the SQD, χ_{SQD}, as a function of the detuning $\hbar\delta$ of the applied field, for an epitaxial system with parameters $a = 10$ nm, $\hbar/T_2 = 2$ meV, $\hbar\omega_0 = 1.546$ eV, $\varepsilon_{\mathrm{env}} = \varepsilon_{\mathrm{S}} = 12\varepsilon_0$ and $\mu = 0.6e$ nm, for several values of the interparticle distance: $R = 14$ nm (solid curve), 18 nm (dotted curve), 25 nm (dashed curve) and 80 nm (dashed–dotted curve).

certain range of detunings, to the right of the absorption peak. This is easily explained from the expression of the minimum value of the absorption coefficient (see equation (18)) where we observe that no matter what the values of all parameters of the equation, it gets a negative value. We note, however, that for large interparticle distance the gain becomes practically zero. The negative value of the imaginary part of the SQD susceptibility means that we have gain in this frequency region. Its origin lies in the coherent interaction between the SQD and the plasmons that are induced on the surface of the MNP, and the induced energy transfer between the MNP and the SQD due to this interaction. The systematic study reveals that the increase of the interparticle distance R shifts the absorption resonance frequency to higher values. If we take into consideration the modification of the different parameters as the interparticle distance increases, we conclude that this zero point moves towards lower values of the detuning for small values of center-to-center distance R. However, for higher values of it the zero point once again starts moving to higher δ. In the special case where the two nanoparticles are far away from each other, the gain peak practically extinguishes. Moreover, the gain peak, depicted in more detail in figures 2(c) and 5(c), reaches its highest value at about $R = 16.5$ nm (solid curve in figure 5(c)). For even lower or higher values of the interparticle distance, the gain peak is weaker and the region of the detuning for which we observe gain is narrower.

All features observed related to the position and the value of the imaginary part of the SQD susceptibility can be understood in terms of the behavior of the imaginary part of G and κ-parameters. Our results have shown that G_{I} and the factor containing the real and imaginary part of κ in equation (16), i.e. $\frac{[\kappa_{\mathrm{R}}^2+\kappa_{\mathrm{I}}^2]^{1/2}+\kappa_{\mathrm{R}}}{\kappa_{\mathrm{I}}}$, are decreasing and increasing functions of R, respectively. These opposite trends explain

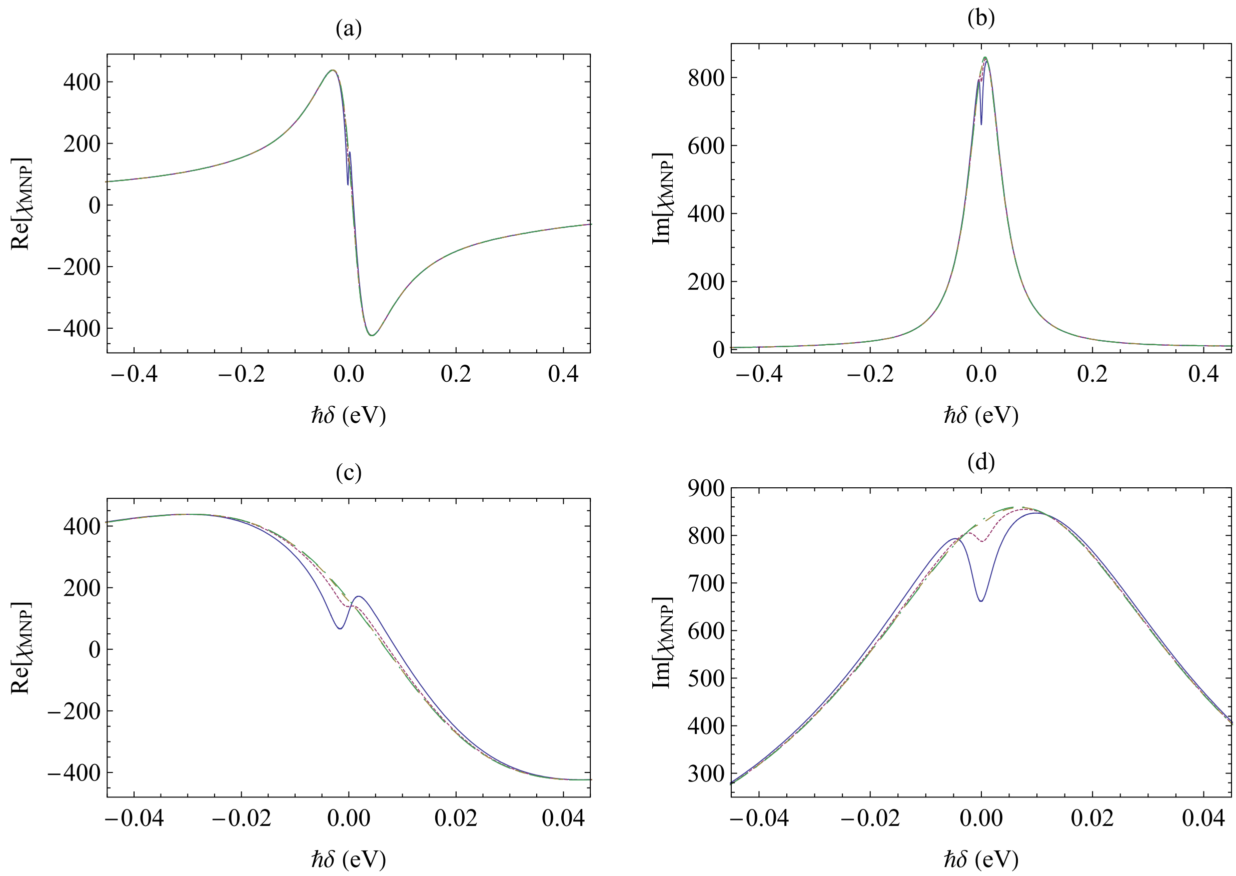

Figure 9. The spectral form of the real, (a) and (c), and imaginary part, (b) and (d), of χ_{MNP} as a function of the detuning $\hbar\delta$ of the applied field for the same parameters as in figure 8. The interparticle distance is $R = 14$ nm (solid curve), 18 nm (dotted curve), 25 nm (dashed curve) and 80 nm (dashed–dotted curve).

why we get an optimal value for the negative imaginary part of the SQD susceptibility (see equation (18)) and why the minimum value occurs at very high detuning at the two limits, i.e. very low and very high separations of the SQD–MNP. In fact, at interparticle distance at around 20 nm, G_{I} and $\frac{1}{T_2}$ have almost the same value and after $R = 30$nm G_{I} is much smaller than $\frac{1}{T_2}$ which makes the term $2(\frac{1}{T_2} + G_{\mathrm{I}})$ an R-independent term.

To obtain a complete picture of the interplay between the excitons of the SQD and the plasmons of the MNP we study in figures 3(b), 6(b) and (c) the imaginary part of the susceptibility of the MNP. It becomes obvious that the coefficient Im $[\chi_{\mathrm{MNP}}]$ gets negative values for a very narrow range of distances R (see dotted curve in figure 6(c) where $R = 20$ nm). This is explained by equation (20) where, for the system under investigation, we observe that the first part of Im$[\chi_{\mathrm{MNP}}]$ is positive and independent of R and the second part is negative and R-dependent.

However, it is very important to note that even for the cases showing a negative imaginary part of the susceptibility of the SQD and the MNP, the imaginary part of the total susceptibility is positive, as it should be due the conservation of the energy in the system. Even in the cases where both SQD and MNP susceptibilities exhibit negative values (see for example the dotted curves in figures 6(c) and 5(c)), the total susceptibility is positive as these features occur at different values of detuning. Moreover, a systematic study of the imaginary part of the total susceptibility (see figures 4 and 7) shows that it is always positive. As we observe in equation (22) one part of Im$[\chi^{(1)}]_{\min}$ is positive and independent of R, as γ_{1I} is a function of only the detuning, and the second part is negative and R-dependent, as G_{I}, χ^0_{MNP} and all κ-parameters are functions of R. By taking the derivative of the R-dependent part of the total susceptibility (equation (22)) we find that the largest absolute value of the second R-dependent part occurs for $R \sim 16$ nm. The value we get is 1.4 and hence the imaginary part of the total susceptibility is positive and equal to 0.96.

In figures 8–10, we investigate the impact of the interparticle distance on the linear susceptibilities for a set of parameters that correspond to an epitaxial SQD–MNP(Au) at a low temperature regime [12]. Here, the radius a of the MNP is equal to 10 nm, the decay and dephasing times are $T_1 = T_2/2$ and $\hbar/T_2 = 2$ meV respectively and the gap between the two energy levels is $\hbar\omega_0 = 1.546$ eV, where the plasmon peak of the MNP occurs when it is embedded in a high refractive index material. Furthermore, the dielectric constants of the environment and the SQD are $\varepsilon_{\mathrm{env}} = \varepsilon_{\mathrm{S}} = 12\varepsilon_0$ and the electric dipole matrix element is $\mu = 0.6e$ nm, as in [12]. These parameters correspond to epitaxial SQD (typically GaAs/AlGaAs). In this case, the characteristics of the curves show a significant change from those of the system

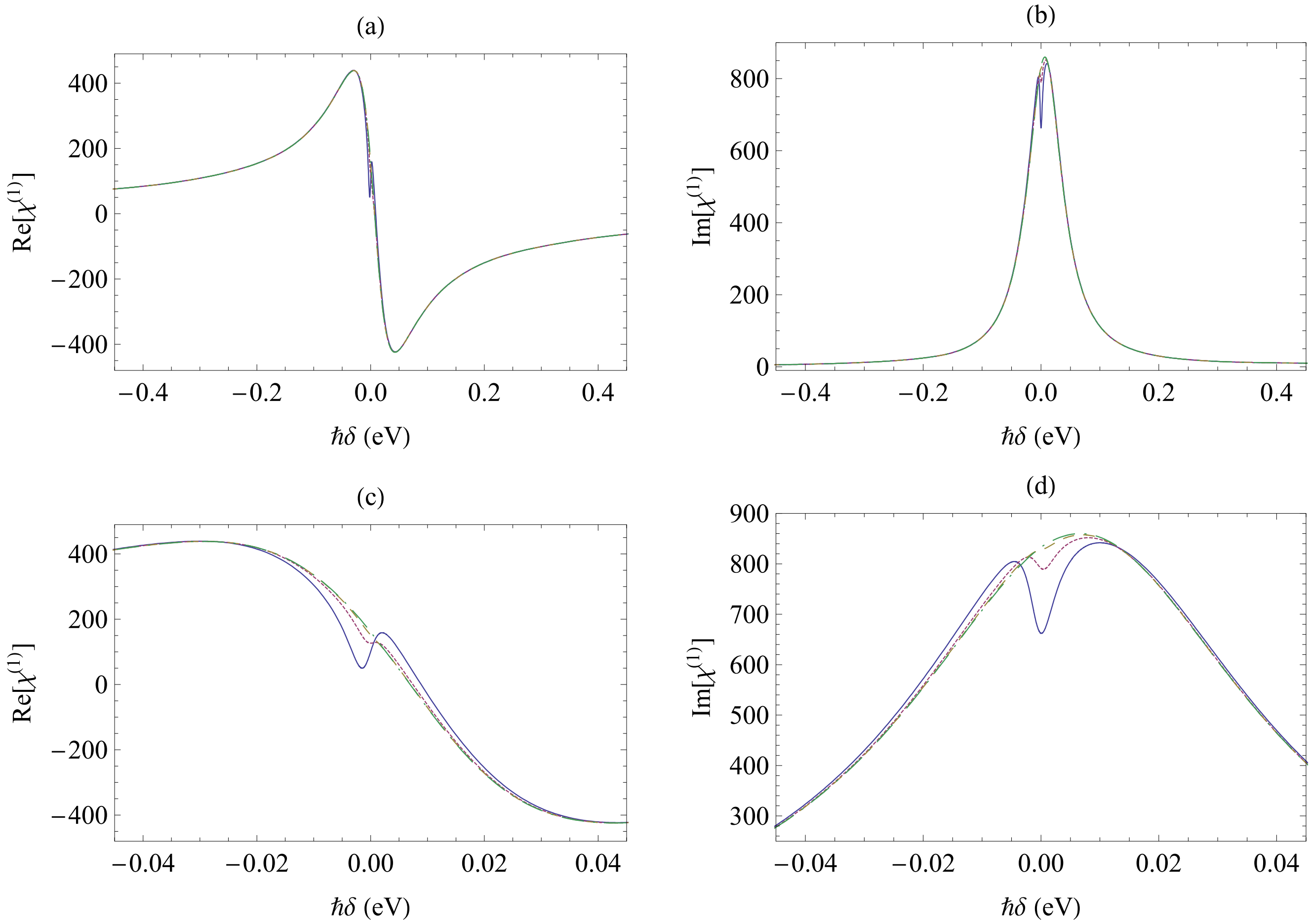

Figure 10. The spectral form of the real, (a) and (c), and imaginary part, (b) and (d), of $\chi^{(1)}$ as a function of the detuning $\hbar\delta$ of the applied field for the same parameters as in figure 8. The interparticle distance is $R = 14$ nm (solid curve), 18 nm (dotted curve), 25 nm (dashed curve) and 80 nm (dashed–dotted curve).

studied previously. Here, the dispersion and the absorption curves have a Fano-type shape. The functional form of the Fano resonance is $\frac{(\delta - q_{\mathrm{Fano}}\Delta_{\mathrm{int}})^2}{\delta^2+\Delta_{\mathrm{int}}^2}$ (plus a negative constant), where Δ_{int} is the interaction-induced broadening and q_{Fano} is the Fano factor. First, we note that for all cases studied (i.e. for various distances) the curves corresponding to the real and imaginary part of the linear susceptibility χ_{SQD} can be fitted by an interaction broadening (Δ_{int}), that takes values in the range between 1 meV and 3 meV. This reveals, as expected, that the most important contribution on the broadening comes from the dephasing time T_2 (as $\hbar/T_2 = 2$ meV) and not from the G-parameter, which for both the real and imaginary part always shows values less than 0.1 meV. In addition, the dimensionless parameter q_{Fano} that corresponds to the physical quantities Re[χ_{SQD}] and Im[χ_{SQD}] takes values in the region 0.3–2.

Figure 9 of the MNP susceptibilities and figure 10 of the total susceptibility reveal that the response of the SQD–MNP hybrid system to the external field is different when compared to the previous one studied in figures 2–7. Here, very broad dispersion and absorption spectra are found, which are only modified for a frequency region of a few meV near zero detuning due to the presence of the SQD. The findings here also confirm that the imaginary part of the susceptibility of the total system never becomes negative.

Before closing this section, we mention that we have also studied the influence of the SQD dipole orientation with respect to the MNP surface to the presented results, as it is well known that this has an important role in the interaction of SQD–MNP systems; see for example [11, 12, 14, 22, 29]. In the present results different SQD dipole orientations lead to different quantitative results; however the qualitative features of the above results remain unchanged. In addition, we have studied the influence of different dielectric constants of the environment on the results and found that they have a small influence on the reported spectra, so the results presented above are still valid.

4. Summary

We studied theoretically optical phenomena in a hybrid system composed of an SQD and a spherical MNP that interacts with an electromagnetic field. For the theoretical analysis we used modified nonlinear density matrix equations. These equations also contain terms which describe the interaction between excitons and surface plasmons. We take the steady state limit of the density matrix equations and obtain a closed-form expression for the linear susceptibilities of the SQD, the MNP and the total system. We investigate the susceptibility dependence on the interparticle distance as well as on material parameters of the hybrid system. We find that the linear optical susceptibility of the SQD leads to an absorption spectrum that is not Lorenzian. The absorption spectrum of the SQD can become zero for specific frequencies and exhibit gain without inversion for a range of frequencies. In addition, we show that the linear susceptibility of the MNP is strongly influenced by the presence of the SQD. Both the SQD and the MNP have a significant contribution in the optical properties of the hybrid system. In all the cases studied the total optical susceptibility leads to an always positive imaginary part, even in cases where both the SQD susceptibility and the MNP susceptibility are negative for different regions of the spectrum. Finally, one can extend the present formalism for calculating the nonlinear Kerr effect or higher order susceptibilities. This can be done by properly using the methodology of [30]. We intend to do this in a forthcoming work.

Acknowledgments

EP would like to thank Dr Garnett W. Bryant for useful communication and for sharing a paper prior to publication.

References

[1] Cheng M-T, Liu S-D, Zhou H-J, Hao Z-H and Wang Q-Q 2007 *Opt. Lett.* **32** 2125
[2] Sadeghi S M 2009 *Nanotechnology* **20** 225401
Sadeghi S M 2009 *Phys. Rev.* B **79** 233309
[3] Sadeghi S M 2010 *Nanotechnology* **21** 355501
Sadeghi S M 2010 *Phys. Rev.* B **82** 035413
[4] Ridolfo A, Di Stefano O, Fina N, Saija R and Savasta S 2010 *Phys. Rev. Lett.* **105** 263601
[5] Waks E and Sridharan D 2010 *Phys. Rev.* A **82** 043845
[6] Malyshev A V and Malyshev V A 2011 *Phys. Rev.* B **84** 035314
[7] Lu Z and Zhu K-D 2009 *J. Phys. B: At. Mol. Opt. Phys.* **42** 015502
[8] Sadeghi S M 2010 *Nanotechnology* **21** 455401
[9] Li J-B, Kim N-C, Cheng M-T, Zhou L, Hao Z-H and Wang Q-Q 2012 *Opt. Express* **20** 1856
[10] Li J-J and Zhu K-D 2011 *Phys. Rev.* B **83** 245421
[11] Zhang W, Govorov A O and Bryant G W 2006 *Phys. Rev. Lett.* **97** 146804
[12] Yan J-Y, Zhang W, Duan S-Q, Zhao X-G and Govorov A O 2008 *Phys. Rev.* B **77** 165301
[13] Artuso R D and Bryant G W 2010 *Phys. Rev.* B **82** 195419
[14] Artuso R D and Bryant G W 2008 *Nano Lett.* **8** 2106
[15] Sadeghi S M and West R G 2011 *J. Phys.: Condens. Matter* **23** 425302
[16] Sadeghi S M, Deng L, Li X and Huang W-P 2009 *Nanotechnology* **20** 365401
[17] Govorov A O 2010 *Phys. Rev.* B **82** 155322
[18] Govorov A O, Fan Z Y, Hernandez P, Slocik J M and Naik R R 2010 *Nano Lett.* **10** 1374
[19] Artuso R D, Bryant G W, Garcia-Etxarri A and Aizpurua J 2011 *Phys. Rev.* B **83** 235406
[20] Hatef A, Schindel D G and Singh M R 2011 *Appl. Phys. Lett.* **99** 181106
[21] Hatef A, Sadeghi S M and Singh M R 2012 *Nanotechnology* **23** 205203
[22] Kosionis S G, Terzis A F, Yannopapas V and Paspalakis E 2012 *J. Phys. Chem.* C **116** 23663
[23] Gersten J and Nitzan A 1981 *J. Chem. Phys.* **75** 1139
[24] Chang D E, Sørensen A S, Hemmer P R and Lukin M D 2006 *Phys. Rev. Lett.* **97** 053002
[25] Trugler A and Hohenester U 2008 *Phys. Rev.* B **77** 115403
[26] Yannopapas V, Paspalakis E and Vitanov N V 2009 *Phys. Rev. Lett.* **103** 063602
[27] Chang-Hasnain C J, Ku P-C, Kim J and Chuang S-L 2003 *Proc. IEEE* **91** 1884
[28] Johnson P B and Christy R W 1972 *Phys. Rev.* B **6** 4370
[29] Vladimirova Y V, Klimov V V, Pastukhov V M and Zadkov V N 2012 *Phys. Rev.* A **85** 053408
[30] Dolgaleva K, Boyd R W and Sipe J E 2007 *Phys. Rev.* A **76** 063806